


X-ray magnetic circular dichroism and neutron diffraction measurements of the magnetic moment of titanium in $\text{Sm}(\text{Fe}_{0.8}\text{Co}_{0.2})_{11}\text{Ti}$

Hiroyuki Suzuki (鈴木 啓幸) ^{*}

Magnetic Materials Research Laboratory, Hitachi Metals, Ltd., 5200 Mikajiri, Kumagaya, Saitama 360-8577, Japan

Akira Nambu (南部 英) and Masakuni Okamoto (岡本 政邦)

Research & Development Group, Hitachi, Ltd., 2520 Akanuma, Hatoyama, Saitama 350-0395, Japan



(Received 1 August 2019; revised manuscript received 7 October 2019; published 30 October 2019)

The magnetic moment of titanium in $\text{Sm}(\text{Fe}_{0.8}\text{Co}_{0.2})_{11}\text{Ti}$ was evaluated directly with x-ray magnetic circular dichroism, and magnitude of titanium's magnetic moment was identified with powder neutron Rietveld analysis. It was demonstrated experimentally that titanium in $\text{Sm}(\text{Fe}_{0.8}\text{Co}_{0.2})_{11}\text{Ti}$ has a magnetic moment of about $1\mu_{\text{B}}$, and that magnetic moment of titanium couples antiferromagnetically to those of the host elements (iron and cobalt) at room temperature. From first-principles calculation, the magnitude of titanium's magnetic moment could be explained by Friedel's concept of the virtual bound state and reverse spin extended to the neighboring iron sites.

DOI: [10.1103/PhysRevB.100.144443](https://doi.org/10.1103/PhysRevB.100.144443)

I. INTRODUCTION

An iron-rich compound including rare-earth elements (R) such as a ThMn_{12} structure ($R\text{Fe}_{12}$) is a promising matrix phase of permanent magnets with high performance. Stabilizing elements (M) such as titanium (Ti) are necessary for the $R\text{Fe}_{12}$ to generate as an equilibrium phase, though its magnetization decreases greatly [1,2]. It can be considered that if a compound based on $R\text{Fe}_{12}$ could be fabricated, it would have high magnetization. Recently, it was reported that $\text{Sm}(\text{Fe}_{0.8}\text{Co}_{0.2})_{12}$ fabricated by a thin-layer method has very high magnetization (1.78 T) at room temperature (RT) [3], while the titanium-substituted compound $\text{Sm}(\text{Fe}_{0.8}\text{Co}_{0.2})_{11}\text{Ti}$ (as shown in Fig. 1) has magnetization of 1.42 T at RT [4]. Moreover, it was revealed that similar Ti-lean compounds also have high magnetization [5–10]. Substitution of iron with cobalt plays the role of increasing Curie temperature (T_{C}) and magnetization [11,12], because the preference of cobalt for the $8f$ site increases the number of electrons in the local majority band of the $8f$ site, and an effect observed in the Slater-Pauling curve is provoked. These compounds with high T_{C} over 750 K are appropriate for the high-temperature-driven motors used in electric vehicles (EVs). It is significant practically to verify magnetic moments of each site changed by substituting M elements. Especially, magnetization of the M elements is not definitive experimentally because there is little direct experimental evidence of their magnetic moments and their directions. They are often treated as nonmagnetic ones in neutron diffraction analysis [13,14]. As a few experimental examples including similar compounds, the magnetic moment of vanadium coupling antiferromagnetically to that of iron could be detected in $\text{Nd}(\text{Fe}, \text{V})_{12}$ and Fe-V alloys by x-ray

magnetic circular dichroism (XMCD) measurements [15]. Moreover, it was confirmed that Ti in $\text{Nd}_3(\text{Fe}, \text{Ti})_{29}$ has a net magnetic moment of unknown strength [16]. On the other hand, the magnetic moments of M elements are interpreted based on the virtual bound states (VBSs) theory by Friedel [17]. Magnetic moments of alloys with a filled majority band, which are called “strong ferromagnets,” can be explained by the alloys' composition via the total number of electrons without considering precise band structures. Since the $R\text{Fe}_{12}$ can be mostly regarded as the strong ferromagnet, strictly, a few unoccupied states remain in the local majority band of the $8f$ site [18], it should be understood by the VBS theory, as shown in Fig. 2. In the case of substituting elements preceding (in the periodic table) the host element of the alloy, M_{pre} hereafter, while each $3d$ level of the elements locates above the Fermi level (E_{F}) in the majority band, it hybridizes due to overlap in the minority band. M_{pre} therefore have magnetic moments aligned antiferromagnetically to those of the host element, whereas, when substituting elements succeeding the host element, M_{suc} hereafter, each $3d$ level of the elements locates under E_{F} in both the majority and minority bands, and the number of unpaired electrons remains almost unchanged.

Thus, it is significant to know whether M elements have magnetic moments or not in $R\text{Fe}_{12}$ and determine the strength of them experimentally. We evaluated the magnetic moment of titanium directly by using x-ray magnetic circular dichroism (XMCD), and we identified the strength of the magnetic moment by Rietveld analysis based powder neutron diffraction. Moreover, estimated magnetic moments were verified by utilizing a first-principles calculation, and magnetization reduction was investigated minutely.

II. EXPERIMENT AND CALCULATION METHODS

Samples prepared using 99.9 + % grade materials (at natural-abundance ratio) were fabricated by rapid quenching

^{*}Present address: Research & Development Group, Hitachi, Ltd., 2520 Akanuma, Hatoyama, Saitama 350-0395, Japan; hiroyuki.suzuki.ke@hitachi.com

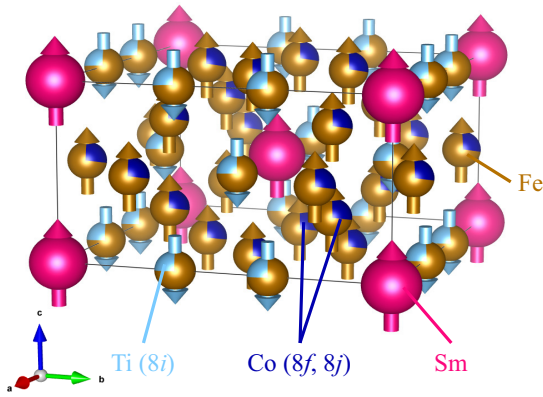


FIG. 1. Crystal structure and directions of magnetic moments of $\text{Sm}(\text{Fe}_{0.8}\text{Co}_{0.2})_{11}\text{Ti}$ at RT.

for composition uniformity, and the thickness of the formed samples was 30–40 μm . After being annealed at 1373 K for 0.3 h in an argon atmosphere, the samples mostly consisted of single phase, and crystallites with size of a few microns were observed by polarizing microscope. The ribbon-formed sample embedded in an epoxy resin was used for XMCD measurement after polishing its surface to eliminate oxidations with thickness of a few microns generated by the annealing, while the powders pulverized to a size of under 75 μm were used for neutron diffraction measurements due to neutrons' high transmission.

XMCD spectra of iron, cobalt, and titanium were obtained at BL-16A of the Photon Factory (PF) in Tsukuba, Japan. As soon as the polished samples were sputtered by argon bombardment, x-ray-absorption spectra (XAS) of iron, cobalt, and titanium taken with opposite x-ray helicities μ_{\pm} were measured at RT under a vacuum of 10^{-5} Pa and a magnetic field of 1 T applied at an angle of 45° along the sample surface. While XMCD of cobalt and titanium were measured by utilizing partial fluorescence yield (PFY), which detects signals from regions a few micron under the sample surface, XMCD of iron was measured by using total electron yield (TEY), which is sensitive to regions a few nanometers below the sample surface, due to a self-absorption.

Neutron diffraction spectrum of the time of flight (TOF) was measured at RT by using iMATERIA specialized powder

diffraction, which is installed at the Material and Life Facility (MLF) in Tokai, Japan. To compensate thermal neutron absorption of samarium, the powder samples were set in a cylindrical, hollow vanadium vessel with outer and inner diameters of 30 and 28 mm, respectively. Total number of scattering neutrons amounts to 79 M counts. Wavelength dependence of incident neutron intensity from nuclear spallation reaction was corrected by vanadium incoherent scattering. The spectrum within the d range from 2.5 to 0.5 \AA collected by a back scattered bank of iMATERIA was analyzed by using the Z code 1.0.2 [19,20]. Since peaks of high scattering vector Q could be measured, Debye-Waller factors were treated as anisotropic ones.

The first-principles calculations were based on the density functional theory in the generalized gradient approximation (GGA). The first-principles electronic-structure code VASP, which uses a plane-wave basis set and a projector augmented wave (PAW), was used for magnetic moments. We also considered structural relaxation, though first-principles calculation of nonstoichiometric composition is better with the Korringa-Kohn-Rostoker (KKR) method with coherent potential approximation (CPA) function [21,22]. The plane-wave cutoff energy was set to 500 eV. $6 \times 6 \times 6$ k points in the Brillouin zone were integrated. The Sm- f states were treated as frozen core with valency of 3. Crystal structures based on $R\text{Fe}_{12}$ were optimized in terms of both their unit cells and atom positions.

III. RESULTS AND DISCUSSIONS

XAS taken with opposite x-ray helicities and XMCD spectra of (a) iron, (b) cobalt, and (c) titanium, and (d) a comparison between XAS of titanium taken by using TEY and PFY are shown in Fig. 3. XMCD spectra were calculated as the difference between two XASs (displayed in each upper figure). Opposite direction peaks of L_{II} and L_{III} edges each corroborate the XMCD signals. Peaks indicated by yellow arrows are assigned to metal components, while peaks indicated by gray arrows are assigned to oxide components judging from chemical shifts. It is worth noting that the XMCD signals of titanium measured by using TEY displayed in (d) come from the oxides and correspond to Ti^{2+} and Ti^{4+} typically. Since the XMCD signals of titanium from the metal

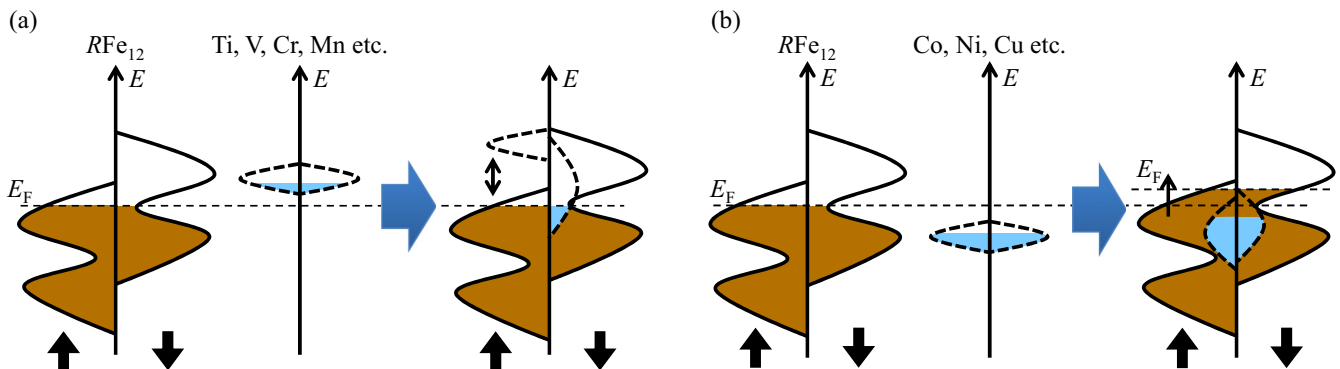


FIG. 2. Schematic illustrations of density of states in the case of substituting elements (a) preceding and (b) succeeding the host element in $R\text{Fe}_{12}$.

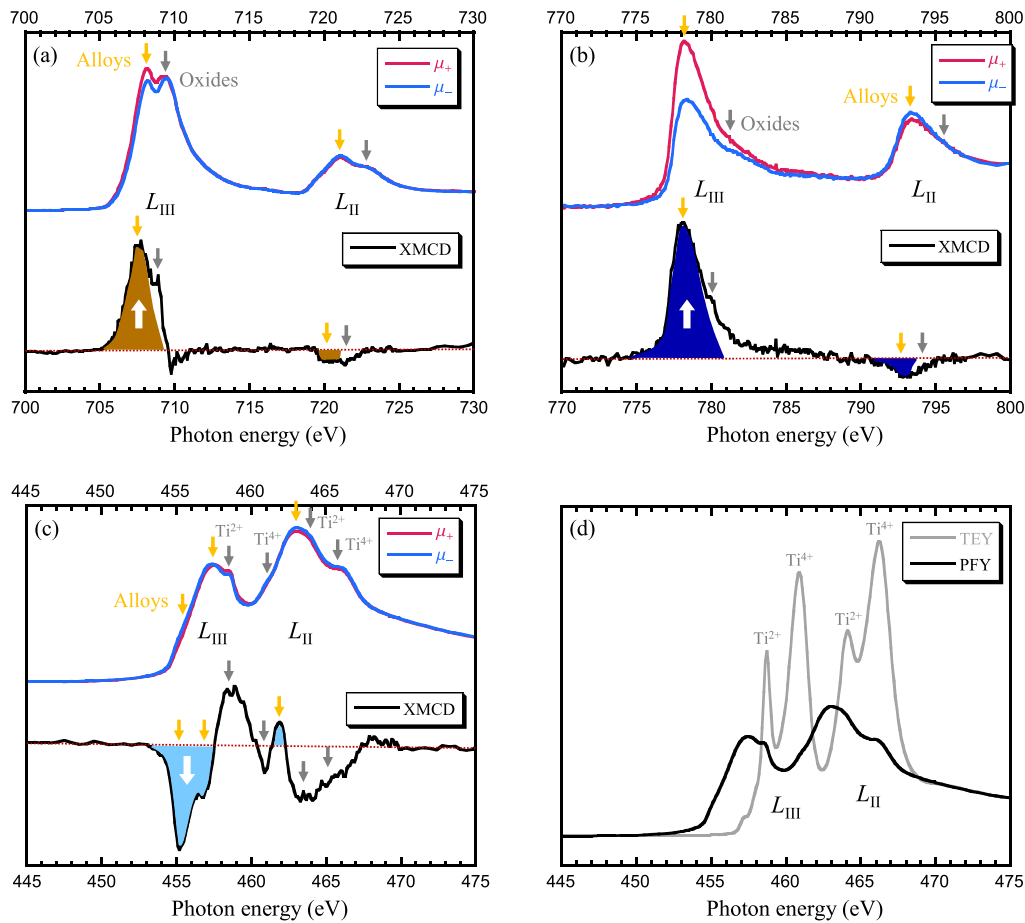


FIG. 3. XAS taken with opposite x-ray helicities and XMCD spectra of (a) iron, (b) cobalt, and (c) titanium, and (d) comparison between XAS of titanium taken by using TEY and PFY.

components were detected in the opposite direction to those of iron and cobalt, it was demonstrated that titanium has a magnetic moment, which was directed in the opposite direction to those of iron and cobalt. This is an experimental demonstration that a magnetic moment coupled antiferromagnetically to those of the host elements is generated at titanium in an iron-based ThMn_{12} structure. Orbital and spin components of the alloy could not be calculated by using the sum rule because the regions attributed to the XMCD signals of the metal and oxide components could not be divided clearly. However, the larger integrated area of the L_{III} edge than that of the L_{II} edge demonstrates that orbital moments survive in any element. It is suggested that $\text{Sm}(\text{Fe}_{0.8}\text{Co}_{0.2})_{11}\text{Ti}$ has a strong anisotropy originated from an iron-based lattice without samarium.

A neutron diffraction pattern fitted by Rietveld analysis (assuming a ferrimagnet) is shown in Fig. 4, and verified structure parameters are tabulated in the inset. It should be noted that almost no nuclear diffractions from samarium are caused by strong neutron absorption of ^{149}Sm . The diffraction comes from a lattice of iron, cobalt, and titanium only. It was demonstrated that titanium prefers the $8i$ site, which corresponds to a dumbbell-type site, while cobalt does not prefer that site, which is the same as the past neutron diffraction results [13,14]. In comparison with the fitting result of the ferrimagnetic model and that of a nonmagnetic

titanium model, the fitting-reliability factor of weighted pattern R_{wp} reduced to 7.31% from 7.44%, and expected R_e values are almost the same, where these values are displayed as $R_{\text{wp}} = \sqrt{\sum_i^N w_i [y_i - f_i(x)]^2 / \sum_i^N w_i y_i^2}$ and $R_e = \sqrt{N / \sum_i^N w_i y_i^2}$ [w_i is the statistical weight, y_i and $f_i(x)$ are observation and theoretical diffraction intensity, respectively, and N and P are the number of data and refined parameters, respectively]. Therefore, the ferrimagnetic model was more suitable than the model that treated titanium as a nonmagnetic element. Since the interaction between atoms in the dumbbell-type site is stronger than that between any other atoms, it is possible to conclude that antiferromagnetic alignment between magnetic moments of titanium and iron is isolated from alignments of other atoms.

The magnetic moments estimated experimentally were verified by first-principles calculations. When dealing with $\text{Sm}(\text{Fe}_{0.8}\text{Co}_{0.2})_{11}\text{Ti}$ in VASP, we approximate nonstoichiometric composition $\text{Sm}(\text{Fe}_{0.8}\text{Co}_{0.2})_{11}\text{Ti}$ with $\text{SmFe}_9\text{Co}_2\text{Ti}$, and for the total arrangement of two cobalt atoms ($_{11}\text{C}_2 = 55$ cases) when titanium is occupied at the $8i$ site, the first-principles calculations including structural relaxation were performed. Four arrangements in which a cobalt atom enters each $8f$ site and $8j$ site were obtained as the lowest arrangement of total energy. The magnetic moments at each site were averaged for these four Co-Fe configurations. Thus, magnetic

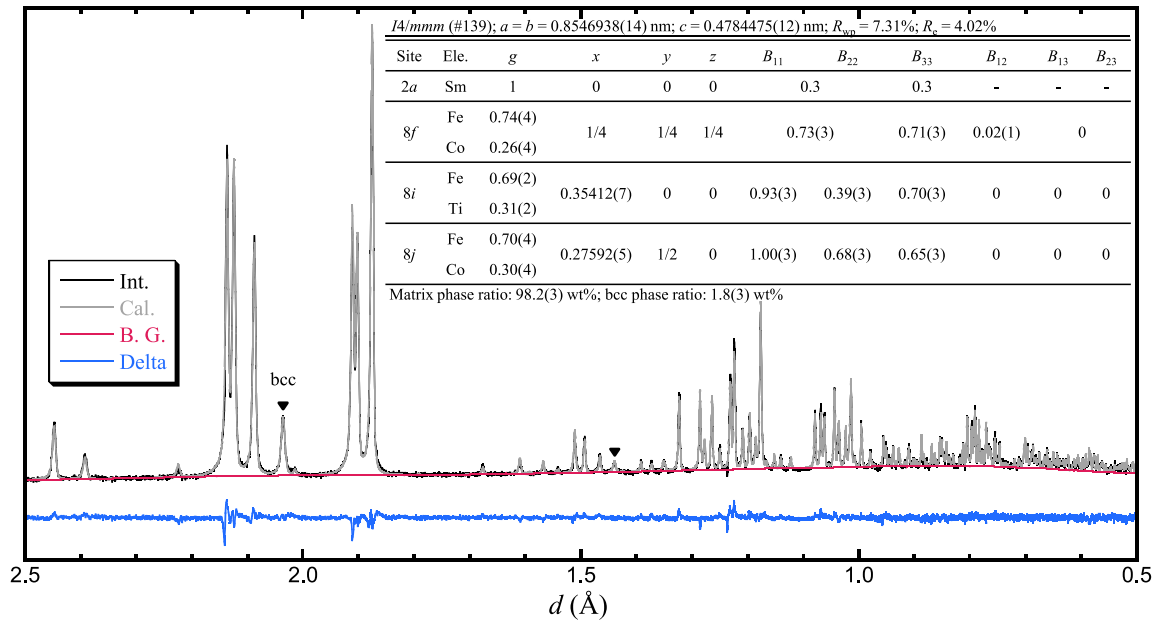


FIG. 4. Neutron diffraction patterns and fitting results by Rietveld analysis assuming an antiferromagnet and verified structure parameters tabulated in an inset.

moments estimated by neutron Rietveld analysis and those calculated by the first principles are compared in Table I. The magnetic moments estimated experimentally have an error of about $0.2\mu_B$. Among the iron sites, the *8i* site has the largest magnetic moment ($2.36\mu_B$), and the *8f* site has the smallest ($1.31\mu_B$). The largest magnetic moment among the iron sites has $2.36\mu_B$ of the *8i* site, and the smallest one has $1.31\mu_B$ of the *8f* site. Magnetic moments of each site estimated by Rietveld analysis largely agree with those calculated by first principles. A large difference between the magnitudes of the magnetic moments at the *8f* site comes from underestimating the magnetic moments in the neutron diffraction experiment, which is correlated with the ambiguity of site occupancies of cobalt. Hence, the magnetization estimated by the experiment (1.29 T) is lower than that estimated by magnetization measurements (1.42 T). However, since the order of the magnetic moments determined by the experiment is the same as that determined by the calculation, the estimation accuracy can be considered reasonable. It is thus concluded that titanium has a magnetic moment with the magnitude of about $1\mu_B$ at RT.

Reduction in magnetization by adding titanium is mainly due to antiferromagnetic coupling between titanium atoms and the iron lattice. It, however, cannot be explained by the antiferromagnetic coupling between titanium, iron, and

TABLE I. Comparison between magnetic moments estimated by the neutron Rietveld analysis and the first-principles calculation.

Methods	8 <i>f</i>		8 <i>i</i>		8 <i>j</i>		Magnetization	
	Fe	Co	Fe	Ti	Fe	Co	(μ_B /f.u.)	(T)
Expt. (300 K)	1.31	0.98	2.36	-1.15	2.25	1.31	19.28	1.29
Calc. (0 K)	2.01	1.39	2.40	-0.80	2.34	1.38	22.58	1.54

cobalt only. By applying Friedel's concept of VBS [17,23], local magnetic moments at titanium sites decrease by $6\mu_B$. To validate the concept, magnetic properties in three cases without cobalt, namely, SmFe_{12} , $\text{SmFe}_{11}\text{Fe}$, and $\text{SmFe}_{11}\text{Ti}$, for simplicity, were calculated from first principles. The calculation results are summarized in Table II. When iron at the *8i* site in SmFe_{12} is substituted by titanium, the unit-cell volume increases about 1.13%, the local magnetic moment at the titanium site decreases about $3.381\mu_B$, and the magnetization M_s decreases about $4.932\mu_B$. The change from SmFe_{12} to $\text{SmFe}_{11}\text{Ti}$ is accomplished by two processes: (i) $\text{SmFe}_{12} \rightarrow \text{SmFe}_{11}\text{Fe}$, which causes an increase in volume, where ΔM_s is about $+0.305\mu_B$; and (ii) $\text{SmFe}_{11}\text{Fe} \rightarrow \text{SmFe}_{11}\text{Ti}$, which causes substitution of titanium, where ΔM_s is about $-5.237\mu_B$. Process (i) is a volume effect in which M_s is increased. Process (ii) is a titanium-substitution effect, which may be explained by Friedel's concept, and M_s is decreased by about $6\mu_B$. Since the difference between theory and calculation is small ($0.763\mu_B$), Friedel's concept is considered to hold. In process (ii), the local magnetic moments of all iron sites decrease. This is due to reverse spin

TABLE II. Summarized calculated magnetic properties. Structures of SmFe_{12} and $\text{SmFe}_{11}\text{Ti}$ are optimized, but the structure of $\text{SmFe}_{11}\text{Fe}$ is the same as that of $\text{SmFe}_{11}\text{Ti}$, in which titanium is substituted by iron.

Compound	Volume (\AA^3)	Magnetization (μ_B /f.u.)	8 <i>f</i>		8 <i>i</i>	
			Fe	Fe	Fe	Ti
SmFe_{12}	169.22	26.3156	1.888	2.365	2.573	
$\text{SmFe}_{11}\text{Fe}$	171.14	26.6204	1.930	2.389	2.594	
$\text{SmFe}_{11}\text{Ti}$	171.14	21.3835	1.807	2.232	2.402	-0.808

(theoretically $-3.406\mu_B$) generated at the titanium sites extending to neighboring iron sites. Therefore, residual spin at the titanium sites is only $-0.808\mu_B$.

IV. CONCLUSIONS

It was determined with XMCD measurements that titanium in the iron-based ThMn_{12} structure has a magnetic moment and the magnetic moment of titanium couples antiferromagnetically with those of the host elements (iron and cobalt) at RT. Neutron Rietveld analysis of $\text{Sm}(\text{Fe}_{0.8}\text{Co}_{0.2})_{11}\text{Ti}$ using a ferrimagnetic structure model demonstrated that the magnetic moment is about $1\mu_B$ at RT. This result was supported by

first-principles calculation. Magnitude of titanium magnetic moment was explained by Friedel's concept of VBS and reverse spin extended to the neighboring iron sites.

ACKNOWLEDGMENTS

This study was performed under the approval of the Photon Factory Program Advisory Committee (Proposal No. 2018C210) and supported by Project No. 2017AM0011 of Ibaraki Prefectural Government. We would like to express our deepest appreciation to Prof. K. Amemiya and Dr. T. Nishiuichi for their support in the XMCD and neutron experiments, respectively.

-
- [1] H.-S. Li and J. M. D. Coey, *Handbook of Magnetic Materials* (Elsevier, Amsterdam, 1991), Vol. 6, Chap. 1, pp. 6–33.
- [2] R. Verhoef, F. R. de Boer, Zhang Zhi-dong, and K. H. J. Buschow, *J. Magn. Magn. Mater.* **75**, 319 (1988)
- [3] Y. Hirayama, Y. K. Takahashi, S. Hirose, and K. Hono, *Scr. Mater.* **138**, 62 (2017).
- [4] P. Tozman, H. Sepehri-Amin, Y. K. Takahashi, S. Hirose, and K. Hono, *Acta Mater.* **153**, 354 (2018).
- [5] S. Suzuki, T. Kuno, K. Urushibata, K. Kobayashi, N. Sakuma, K. Washio, H. Kishimoto, A. Kato, and A. Manabe, *AIP Adv.* **4**, 117131 (2014).
- [6] N. Sakuma, S. Suzuki, T. Kuno, K. Urushibata, K. Kobayashi, M. Yano, A. Kato, and A. Manabe, *AIP Adv.* **6**, 056023 (2016).
- [7] S. Suzuki, T. Kuno, K. Urushibata, K. Kobayashi, N. Sakuma, K. Washio, M. Yano, A. Kato, and A. Manabe, *J. Magn. Magn. Mater.* **401**, 259 (2016).
- [8] T. Kuno, S. Suzuki, K. Urushibata, K. Kobayashi, N. Sakuma, M. Yano, A. Kato, and A. Manabe, *AIP Adv.* **6**, 025221 (2016).
- [9] K. Kobayashi, S. Suzuki, T. Kuno, K. Urushibata, N. Sakuma, M. Yano, T. Shouji, A. Kato, and A. Manabe, *J. Alloys Compd.* **694**, 914 (2017).
- [10] M. Hagiwara, N. Sanada, and S. Sakurada, *J. Magn. Magn. Mater.* **465**, 554 (2018).
- [11] Y.-C. Yang, S. Hong, Z.-Y. Zhang, L. Tong, and J.-L. Gao, *Solid State Commun.* **68**, 175 (1988).
- [12] L. Bessais and C. Djega-Mariadassou, *Phys. Rev. B* **63**, 054412 (2001).
- [13] J. K. Liang, Q. Huang, A. Santoro, J. L. Wang, and F. M. Yang, *J. Appl. Phys.* **86**, 2155 (1999).
- [14] Y.-C. Yang, L.-S. Kong, and H. Sun, *J. Appl. Phys.* **67**, 4632 (1990).
- [15] M. G. Shelyapina, N. E. Skryabina, D. Fruchart, E. K. Hlil, P. Wolfers, and J. Tobola, *Chem. Met. Alloys* **1**, 105 (2008).
- [16] C. Sarafidis, F. Wilhelm, A. Rogalev, M. Gjoka, and O. Kalogirou, *J. Phys.: Condens. Matter* **21**, 236001 (2009).
- [17] J. Friedel, *Nuovo Cimento* **7**, 287 (1958).
- [18] R. Coehoorn, *Phys. Rev. B* **41**, 11790 (1990).
- [19] R. Oishi, M. Yonemura, Y. Nishimaki, S. Torii, A. Hoshikawa, T. Ishigaki, T. Morishima, K. Mori, and T. Kamiyama, *Nucl. Instrum. Methods Phys. Res. A* **600**, 94 (2009).
- [20] R. Oishi-Tomiyasu, M. Yonemura, T. Morishima, A. Hoshikawa, S. Torii, T. Ishigaki, and T. Kamiyama, *J. Appl. Cryst.* **45**, 299 (2012).
- [21] M. Ogura and H. Akai, *J. Comput. Theor. Nanosci.* **6**, 2483 (2009).
- [22] T. Miyake and H. Akai, *J. Phys. Soc. Jpn.* **87**, 041009 (2018).
- [23] Y. Harashima, K. Terakura, H. Kino, S. Ishibashi, and T. Miyake, *J. Appl. Phys.* **120**, 203904 (2016).